Conductance of photons in disordered photonic crystals

A. A. Asatryan, L. C. Botten, M. A. Byrne, T. N. Langtry, and N. A. Nicorovici
Department of Mathematical Sciences, University of Technology, Sydney, New South Wales 2007, Australia

R. C. McPhedran, C. Martijn de Sterke, and P. A. Robinson
School of Physics, University of Sydney, New South Wales 2006, Australia
(Received 10 September 2004; revised manuscript received 12 November 2004; published 28 March 2005)

The conductance of photons in two-dimensional disordered photonic crystals is calculated using an exact multipole–plane wave method that includes all multiple scattering processes. Conductance fluctuations, the universal nature of which has been established for electrons in the diffusive regime, are studied for photons, in both principal polarizations and for varying disorder. Our simulations show that universal conductance fluctuations can be observed in $H_{\|}$ (TE) polarization for weak and intermediate disorder while, for $E_{\|}$ (TM) polarization, we show that the conductance variance is essentially independent of sample size but strongly dependent on disorder. The probability distribution of the conductance is also calculated in the diffusive and localized regimes, and also at their transition, for which the distributions for both polarizations are seen to be very similar.

DOI: 10.1103/PhysRevE.71.036623 PACS number(s): 42.25.Dd, 42.25.Fx

I. INTRODUCTION

The discovery of universal conductance fluctuations (UCF's) of electrons [1], in which the variance of the conductance g does not depend on the size or the degree of disorder of the mesoscopic conductors, has led to considerable research [2] in order to understand the nature of such anomalously large fluctuations. The scaling theory of Anderson localization assumes that the conductance g is determined by its behavior for a system of a given size, with the conductance for systems of any other size being obtained through a scaling function [3]. Since scaling theory is based on the scaling properties of the averaged conductance $\langle g \rangle$, the discovery of UCF's initiated a wide ranging discussion about the validity of scaling theory itself. Indeed, it has been suggested that the scaling theory needs to be reformulated in terms of conductance distributions $p(g)$ [4]. At this time, however, no such theory exists.

The conductance distribution for the electronic case was calculated numerically [5,6] for both insulating and metallic regimes, and also at the mobility edge [7,8]. Subsequently, nonanalytic behavior of $p(g)$ was reported at the crossover point ($\langle g \rangle \approx 1$) [9] for systems without time reversal symmetry. Despite substantial research, however, the characterization of the conductance distribution remains incomplete.

Originally developed to describe the transport properties of electrons in disordered wires, the concept of conductance can also be applied to photons [10]. Calculations of $p(g)$ have been undertaken using a modal approach for surface corrugated waveguides [11,12] while the distribution of the total transmittance has been investigated in the diffusive approximation [13], using random matrix theory [14], and experimentally [15]. In the diffusive regime ($\langle g \rangle \gg 1$) [13], the distribution of the total transmittance is approximately Gaussian, while in the strong scattering regime, the theory [13,14] can be modified to give good agreement with experiment [16].

Diagrammatic techniques [1,10] have provided essential insight into the contribution of different terms of the intensity correlation function for weak disorder. However, the applicability of such expansions to strong disorder is not clear. For this reason, a nonperturbative rigorous method of calculation that takes into account all scattering events is needed. To date, however, none of the models for conductance calculations (for dimensions $d \geqslant 2$) with bulk defects takes into account all multiple scattering events for photons, and nor do existing models incorporate polarization dependence. It is the purpose of this paper to address these deficiencies and to present calculations for conductance fluctuations and the associated probability distributions based on an analytically rigorous method that takes into account all scattering events. While the modeling of noninteracting photons differs from that of electrons, most of the electronic models neglect electron-electron interactions. Accordingly, the results obtained for photons may also be relevant to electrons.

We investigate the conductance fluctuations of photons and their distribution for two-dimensional disordered photonic crystals consisting of high index cylinders arranged in air in a doubly periodic fashion and with their axes parallel to each other. We study their behavior for both principal polarizations—when the electric field ($E_{\|}$) or the magnetic field ($H_{\|}$) is aligned with the cylinder axes. Our calculations are based on the exact method of multipole expansions and rigorously include all scattering events. They combine both a microscopic approach [1] in which the multiply scattered field is calculated exactly for single layers, and a macroscopic approach [17] in which these layers are stacked using exact recurrence relations. We introduce disorder through randomization of the cylinder refractive indices. We then calculate the conductance of the bulk, disordered photonic crystal, investigating the effects of disorder and sample size on the conductance, its fluctuations, and its distribution in the diffusive regime ($\langle g \rangle \gg 1$), in the localized regime ($\langle g \rangle \ll 1$), and at the transition region ($\langle g \rangle \approx 1$).

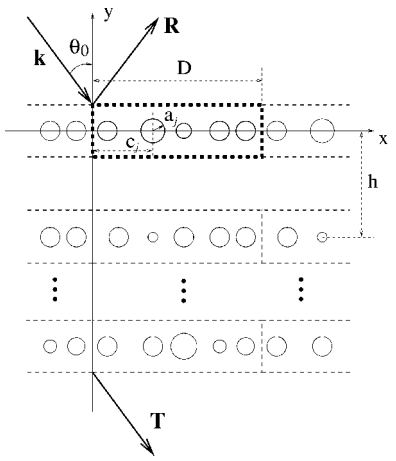

FIG. 1. Diffraction geometry displaying a supercell of a random stack upon which is incident a single plane wave, giving rise to reflected R and diffracted T plane wave orders.

II. COMPUTATIONAL METHOD

We consider a two-dimensional, disordered photonic crystal, each layer of which is a cylinder diffraction grating with a supercell periodically replicated in the x direction (see Fig. 1). The supercell of length D comprises a set of N_c infinitely long cylinders of radii a_j and refractive indices n_j, placed in air with centers located at $\mathbf{x}=\mathbf{c}_j$. The properties of each grating layer are then computed rigorously using a multipole method from which plane wave scattering matrices that characterize the action and interaction of each grating layer are calculated [18]. The fields around each cylinder are expressed in terms of multipole expansions, and we include sufficient terms to have good accuracy (one part in 10^5, or better, for energy calculations) in the solution of the scattering problem for a given grating layer. The quasiperiodic relationship between the fields for cylinders in one period cell and those in other cells is ensured using lattice sums, calculated to high accuracy [18].

The scattering action of an individual grating is parametrized by its period D, and the wavelength $\lambda=2\pi/k$ (in free space) and angle of incidence θ_0 of an incident plane wave field. The diffraction grating equation then defines a sequence of channels p, commonly referred to as diffraction orders, the propagation directions (θ_p) of which are given by $\sin\theta_p=\alpha_p/k$ where $\alpha_p=k\sin\theta_0+2\pi p/D=k\sin\theta_p$. The corresponding direction cosine terms are given by $\cos\theta_p=\chi_p/k$ where $\chi_p=\sqrt{k^2-\alpha_p^2}$ with $\mathrm{Re}(\chi_p)+\mathrm{Im}(\chi_p)>0$. Thus there are a finite number of propagating channels for which $\mathrm{Im}\,\chi_p=0$ and an infinite number of evanescent channels for which $\mathrm{Im}\,\chi_p>0$. In the general scattering problem that we consider, each of the grating orders can represent both an input channel and an output channel. The action of the grating (l) can be characterized by reflection ($\boldsymbol{r}_l$) and transmission ($\boldsymbol{t}_l$) scattering matrices, the elements of which are $r_{pq}^{(l)}$ and $t_{pq}^{(l)}$. In this nomenclature, the term $t_{pq}^{(l)}$ refers to the field amplitude transmitted into an output channel p (with direction sine α_p/k) from a unit amplitude input in channel q. For simplicity, we exploit the treatment in Ref. [18] which normalizes all field amplitudes so that the energy fluxes carried by the propagating diffracted orders can be computed from the square magnitude of the matrix elements, e.g., $|t_{pq}^{(l)}|^2$. We assume, for these calculations, that each grating layer is up-down symmetric and thus its action, for incidence from either above or below, can be characterized by just the two matrices $\boldsymbol{r}_l$ and $\boldsymbol{t}_l$. Finally, the scattering matrices of the individual grating layers are then coupled using recurrence relations to yield the transmission ($\mathbf{T}$) and reflection ($\mathbf{R}$) scattering matrices for a slab of N_L layers [18]. Accordingly, the total transmitted flux through the stack, due to a unit amplitude plane wave field incident in channel q, can be calculated from $g_q=\Sigma_{p\in\Omega_p}|T_{pq}|^2$, with the summation taken over the set of all propagating channels Ω_p.

The dimensionless conductance of the sample is given by the generalized two-terminal Landauer formula [19] for multichannel propagation by summing the aggregate transmittance g_q over each of the possible propagating incident channels q. That is,

$$g=\sum_{q\in\Omega_q} g_q=\sum_{p,q\in\Omega_p}|T_{pq}|^2=\mathrm{Tr}\mathbf{T}\mathbf{T}^\dagger=\mathrm{Tr}\mathbf{T}^\dagger\mathbf{T}, \qquad (1)$$

in which Tr denotes the matrix trace, summed over only the propagating channels (i.e., orders with χ_p real). The matrices $\mathbf{R}$ and $\mathbf{T}$ are infinite in dimension and must be truncated in any numerical implementation, with the truncation order determined by various convergence studies. We retain plane wave orders $[-N_t,N_t]$, ensuring that this set includes all propagating channels, and as many evanescent channels as are required for convergence to be achieved. We choose N_t to be sufficiently large in order to give five significant figures of accuracy, or better, for the elements of the reflection and transmission matrices. The conductance is actually computed by summing the square magnitudes $|T_{pq}|^2$ associated with all propagating input and output channels as in Eq. (1).

Equation (1), the two-terminal Landauer formula for electronic conductance, is derived assuming that the same leads are used to drive the current and to carry out the measurements. There is also a four-terminal form of the Landauer formula [20], in which separate leads are used for the input and output measurements. In the case of photon conductance, the corresponding leads or terminals would be represented, respectively, by the light source and the detector that collects the total transmitted energy. In order to calculate the photon conductance one needs to measure the full transmittance for each incident "energetic" angle (or channel) and then sum (or integrate) these transmittances over every possible incident channel. This experimental configuration would correspond to the two-terminal measurements in the electronic case. Here, we are concerned with a disordered crystal for which a physical experiment requires an extended but finite sample. The full simulation of this, however, is beyond the capacity of current computers and so the modeling is usually undertaken for a truncated structure with periodic boundary conditions, modeled using a supercell. The structure that we model is thus a diffraction grating with a sufficiently large period to allow the diffraction orders to approximate the continuum of directions along which the scattering field is distributed.

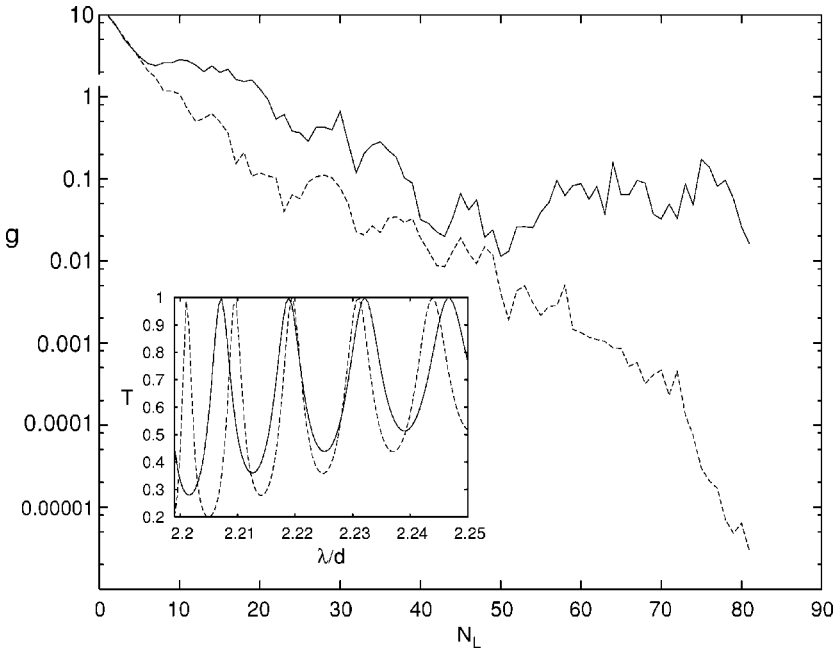

FIG. 2. Conductance g versus the number of layers N_L for a single realization and $Q=0.4$, $\lambda=2.21d$, and $E_\parallel$ polarization. Solid line, evanescent coupling included ($N_t=50$); dashed line, only propagating orders included ($N_t=9$). Inset: transmittance versus wavelength for normal incidence on the stack with 41 identical layers, $Q=0$. The solid line is for $N_c=21$ cylinders per unit cell with the inclusion of the evanescent waves, $N_t=50$, while the dashed line is the same calculation without the evanescent field, $N_t=9$.

While any of the parameters $\mathbf{c}_j$, a_j, and n_j can be randomized, the results here are for random refractive indices n_j, uniformly distributed in the interval $[\overline{n}-Q,\overline{n}+Q]$, where Q is the strength of the disorder. In this calculation we take $N_c=21$. The calculations are undertaken with the family of plane waves associated with a normal incidence configuration ($\theta_0=0$), with either the electric field aligned with the cylinder axes ($E_\parallel$ or TM polarized) or the magnetic field aligned with the cylinder axes ($H_\parallel$ or TE polarized). Throughout, we model a square lattice with lattice constant d, and cylinders of fixed normalized radius $a_l/d=0.3$ and choose $\overline{n}=3$. The wavelength is $\lambda=2.21d$, located in the passband between the first two gaps of the associated regular photonic crystal. There are 19 propagating orders for these parameters and we take $N_t=50$. Unless otherwise stated, averages were calculated over 4900 realizations, sufficient to yield ensemble means stable to approximately two significant figures.

We begin by demonstrating the importance of including sufficient evanescent plane wave terms in the field expansions in order to ensure a well converged solution. In the inset of Fig. 2 we plot the transmission of a stack with $N_L=41$ identical layers with $N_c=21$ identical cylinders per unit cell and $N_t=50$, versus wavelength (solid line). With $N_c=21$, the calculation includes some 101 ($=2N_t+1$) plane waves, only 19 (i.e., $p\in\Omega_p=\{-9,\ldots,9\}$) of which are propagating (i.e., Im $\chi_p=0$), with the remainder evanescent (i.e., Im $\chi_p>0$). The dashed line repeats the calculation, but this time excluding all evanescent terms and including only the 19 propagating waves. The clear difference between the calculations demonstrates the importance of including sufficiently many evanescent terms in the calculation to ensure a well converged result. In the main part of Fig. 2 we show the conductance as a function of stack length N_L for a single realization with the inclusion of sufficient evanescent terms to ensure convergence (solid line), and without evanescent order terms (dashed line). From this, it is clear that the evanescent field is important in accurately characterizing the conductance. Note that in the localized regime ($g\lesssim 1$), the inclusion of evanescent plane wave terms is vital for the accurate characterization of the transport.

III. RESULTS

A. Average of conductance and its fluctuations

We now turn to the study of the average conductance $\langle g\rangle$ and its fluctuations and note that for electrons, in the case of weak disorder, the variance of the conductance

$$\sigma^2=\langle g^2\rangle-\langle g\rangle^2\approx \text{const}, \tag{2}$$

which is independent of both the degree of disorder and the size of the sample—the universal conductance fluctuations [1]. We begin by investigating this phenomenon for photons in the transition from weak to strong disorder for both polarizations.

First, in Fig. 3, we show the dependence of the average conductance $\langle g\rangle$ on the number of layers N_L for weak, moderate, and strong disorder Q in the case of $E_\parallel$ polarization. The maximum stack length is $N_L=81$ and thus, for this length and $N_c=21$, there are 1701 cylinders in each sample. Three wave propagation regimes, which are more prominent for strong disorder (dotted line in Fig. 3), are apparent. The regions where the regimes occur depend on the degree of the disorder Q. The diffusive ($\langle g\rangle>1$) and transition regimes ($\langle g\rangle\approx 1$) occur, respectively, for $N_L\lesssim 10$ and $10\lesssim N_L\lesssim 20$ layers, while for longer stacks ($N_L\gtrsim 20$) the linear behavior (implying exponential decay of the $\langle g\rangle$) points to the onset of Anderson localization. For strong disorder ($Q=1.5$), the transition to Anderson localization requires fewer layers than for weak disorder. According to the Thouless criterion [21], the onset of localization occurs when $\langle g\rangle\approx 1$, while for $\langle g\rangle>1$, waves are delocalized. In Fig. 3, we observe transitions to the linear regime (i.e., localization) commencing at $\langle g$

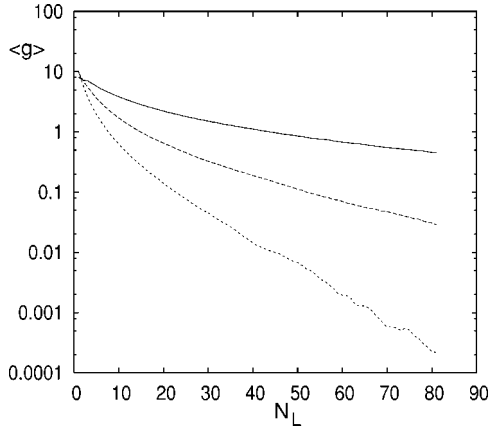

FIG. 3. Average $E_{\|}$ polarization conductance $\langle g \rangle$ versus size of the cluster N_L for different degrees of disorder: $Q=0.2$ (solid line), 0.4 (dashed line), and 1.5 (dotted line).

$\approx 1.5, 0.4, 0.3$, for $Q=0.2, 0.4, 1.5$ respectively—results that are not inconsistent with the Thouless criterion.

Figure 4 shows the variance (σ^2) of the conductance as a function of the number of layers. For weak disorder ($Q=0.2$), σ^2 depends only weakly on the number of layers for $N_L \geqslant 30$ (top curve), while for stack lengths $60 \leqslant N_L \leqslant 70$ the variance is constant to within 2%, with localization appearing for stacks exceeding $N_L \approx 75$. For stronger disorder, the onset of localization, in which the variance decreases with stack length, occurs earlier (i.e., for shorter stack lengths)—results that are similar to those observed in the electronic case [22]. In Fig. 5 we see that the variance σ^2 depends strongly on the disorder Q, with approximately constant conductance fluctuations being observed only in a narrow range of disorder, for $0.15 < Q < 0.2$ and $N_L=15$ (top curve), while for $N_L=40$ the variance of the conductance decreases monotonically for $Q > 0.1$ (bottom curve).

Figure 6(a) is similar to Fig. 3, but this time for $H_{\|}$ polarization. Small oscillations in $\langle g \rangle$, with the number of layers N_L, are now apparent. To determine their origin, we show in the inset of Fig. 6(a) the result of a convergence study, showing the average $\langle g \rangle$ versus the number of realizations. Thus $\langle g \rangle$ is well converged, with the results accurate to two significant figures for 4000 or more realizations. To deduce the physical origin of these oscillations, we considered the variation of $\langle g \rangle$ with stack length (N_L) for both an ordered stack (i.e., $Q=0$) and a weakly disordered stack ($Q=0.2$), shown, respectively, as the upper and lower curves of Fig. 6(b). There is a clear correspondence between the maxima and minima of these curves and we thus conclude that the oscillations of $\langle g \rangle$ in Fig. 6(a) for weak disorder are remnants of Fabry-Pérot resonances associated with reflections from the front and back interfaces of the sample.

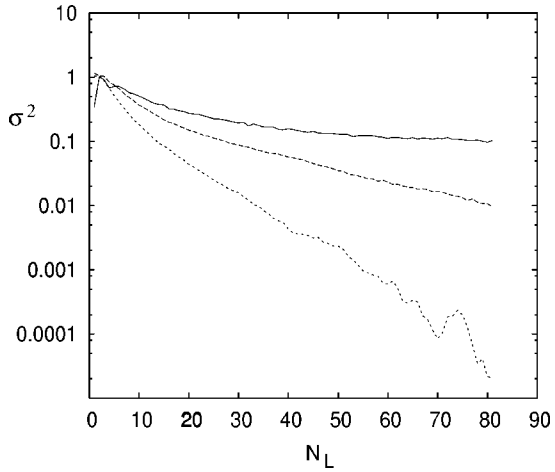

FIG. 4. Variance σ^2 ($E_{\|}$ polarization) versus cluster size N_L for different degrees of disorder: $Q=0.2$ (solid line), 0.4 (dashed line), and 1.5 (dotted line).

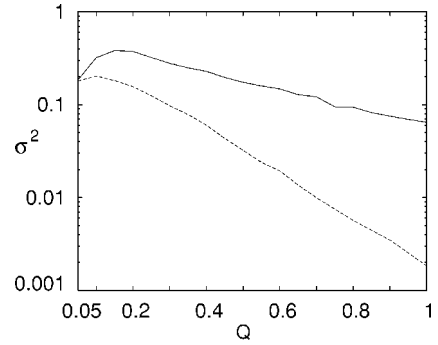

FIG. 5. $E_{\|}$ polarization conductance variance σ^2 versus Q for $N_L=15$ (solid curve) and for $N_L=40$ (dashed curve).

We also compare $\langle g \rangle$ for ordered and very weakly disordered stacks ($Q=0.05$) for $E_{\|}$ polarization and observed the same resonances. The fact that oscillatory behavior is evident only for very weakly disordered stacks for $E_{\|}$ polarization suggests that $\langle g \rangle$ is less sensitive to disorder for $H_{\|}$ polarization than for $E_{\|}$ polarization. This may be interpreted in terms of the stronger scattering by dielectric objects in air that is observed for $E_{\|}$ polarization than for $H_{\|}$ polarization [23] and which is related to the absence of a full band gap in $H_{\|}$ polarization for a photonic crystal composed of dielectric inclusions.

The transition to the linear (localization) regime of Fig. 6(a) for $H_{\|}$ polarization for strong disorder (i.e., $Q=1.5$) occurs for stack lengths $N_L \gtrsim 50$ (corresponding to $\langle g \rangle \lesssim 0.3$).

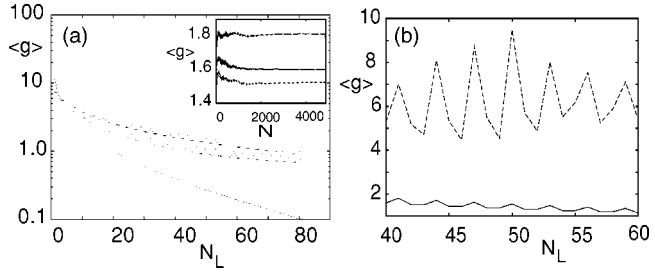

FIG. 6. (a) Average conductance $\langle g \rangle$ for $H_{\|}$ polarization versus cluster size N_L for different degrees of disorder: $Q=0.2$ (solid line), 0.4 (dashed line), 1.5 (dotted line). The inset shows $\langle g \rangle$ vs the number of realizations N for $N_L=40$ (middle curve), 41 (top curve), and 42 (bottom curve). (b) Average conductance $\langle g \rangle$ versus N_L for $Q=0$ (dashed curve) and 0.2 (solid curve).

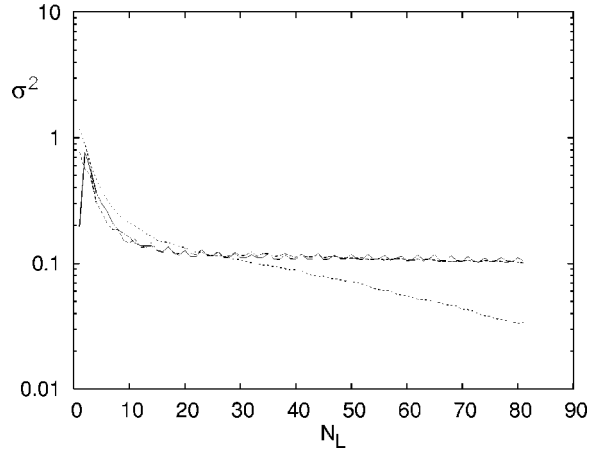

FIG. 7. $H_{\|}$ polarization variance σ^2 vs N_L for different degrees of disorder: $Q=0.2$ (solid line), 0.4 (dashed line), and 1.5 (dotted line) and for $H_{\|}$ polarization.

For weak and moderate disorder (e.g., $Q=0.2,0.4$), however, the transition to the linear regime requires in excess of $N_L=70$ layers.

Figure 7 shows the variance of the conductance for $H_{\|}$ polarization as a function of N_L and reveals that, for weak and moderate disorder ($Q=0.2,0.4$), it depends neither on the length of the stack nor on the disorder. For strong disorder ($Q=1.5$), the variance decreases in a manner similar to that for $E_{\|}$ polarization.

For weak disorder, the calculations for Figs. 3–7, based on a rigorous theory that can handle any range of conductivity or disorder, reveal a substantial plateau in the conductance variance for $H_{\|}$ polarization, and weak dependence on stack length in the case of $E_{\|}$ polarization, with a "plateau" which is flat to within 2% occurring for stacks of 60–70 layers, prior to the onset of localization. It is interesting to observe that the variance, where it is essentially constant, shares the same value of $\sigma^2\approx 0.11$, even when the average conductance $\langle g\rangle \lesssim 1$, i.e., close to the localization regime according to the Thouless condition. Up until now, however, such calculations have been performed using either simplified models or approximate methods such as random matrix theory which, for the electronic case [24], predicts a variance of $\sigma^2=2/15=0.13$ ($\beta=1$), a value slightly larger than our estimate for the photonic case. Implicit in the application of random matrix theory to calculations in the UCF regime is an assumption of diffusive propagation that is normally associated with $g>1$. It is known, however, that the lower bound of the conductance required to observe UCF's lies at the transition from diffusive to localized propagation [24,25] which, in Sec. III B, we show to occur at $g\approx 0.5$. The results in Fig. 7, which show the presence of UCF's for $H_{\|}$ polarization, and also those of Fig. 4 (for $E_{\|}$ polarization) for values of $g<1$, are thus consistent with diffusive propagation extending down to this transition. Finally, we note that the similarity between the computed variance for the photonic ($\sigma^2\approx 0.11$) and electronic ($\sigma^2\approx 0.13$) cases is not surprising since, in two dimensions, the wave propagation equation, in either case, is the Helmholtz equation.

Furthermore, for weak disorder ($Q=0.2$) and appropriately long stacks, we observe that the variance for $E_{\|}$ polarization (Fig. 4), where it is essentially constant, and for $H_{\|}$ polarization (Fig. 7) in the UCF regime has a common value of $\sigma^2\approx 0.11$. Note that to observe this property, the stacks have to be sufficiently long ($N_L>60$) to stabilize the variance at this value, but not long enough for localization to occur. In Fig. 7 we note two strong signatures of UCF's—the coincidence of the results for σ^2 for weak and moderate disorder, and the insensitivity of this quantity to system size. The onset of the region where UCF's are evident is for $N_L\approx 15$, $\langle g\rangle\approx 2$ (Fig. 6).

B. Conductance distributions

In this section we consider the conductance distribution $p(g)$ for both polarizations, and for the three propagation regimes: diffusive ($\langle g\rangle>1$), transition ($\langle g\rangle\approx 1$) and localiza-

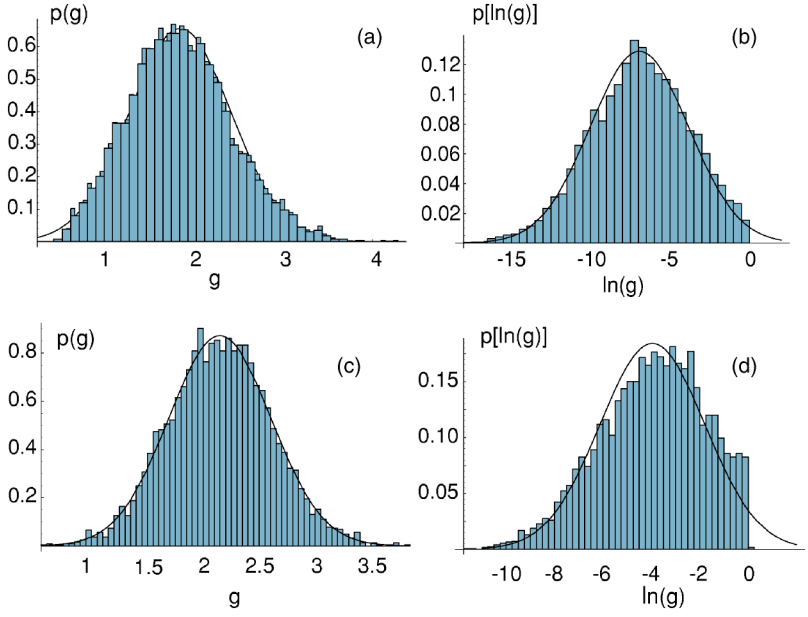

FIG. 8. Conductance distribution $p(g)$ in the diffusive regime ($N_L=10, Q=0.4, \langle g\rangle=1.7$), (a) and the distribution of its logarithm $p(\ln g)$ in the localization regime (b) for $E_{\|}$ polarization ($N_L=81, Q=0.4, \langle g\rangle=0.029$). Graphs (c) ($N_L=10, Q=1.5, \langle g\rangle=2.15$) and (d) ($N_L=10, Q=1.5, \langle g\rangle=0.1$) are similar to (a) and (b), but for $H_{\|}$ polarization. The fitted line is a Gaussian distribution. Fitting was done by using $\langle g\rangle$ and σ calculated from the sample for (a) and (c), and $\langle \ln g\rangle$ and σ for (b) and (d).

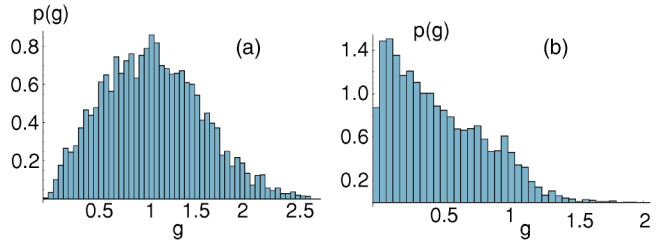

FIG. 9. Conductance distribution $p(g)$ in the transition regime for $E_\parallel$ polarization. (a) $\langle g\rangle=0.98$, $Q=0.4$, $N_L=14$; (b) $\langle g\rangle=0.48$ $Q=0.4$, $N_L=24$.

tion ($\langle g\rangle<1$). For the examples in Figs. 3 and 4, for $E_\parallel$ polarization, weak disorder ($Q=0.2$), and a sufficiently long stack ($N_L=81$), the ensemble means and standard deviations are, respectively, $\langle g\rangle\approx 0.45$ and $\sigma\approx 0.35$. For $H_\parallel$ polarization and the same parameter values, $\langle g\rangle\approx 0.87$ and $\sigma\approx 0.32$. Given the sizes of these standard deviations compared to the means, the first two moments may be insufficient to characterize the full conductance distributions.

As shown in Figs. 8(a) and 8(c) for $E_\parallel$ and $H_\parallel$ polarizations, respectively, the conductance distribution in the diffusive regime is well approximated by a Gaussian distribution

$$p(g)=\frac{1}{\sqrt{2\pi\sigma^2}}\exp\left[\frac{-(g-\langle g\rangle)^2}{2\sigma^2}\right]. \tag{3}$$

We note that this is an approximation since the Gaussian distribution is defined on an infinite interval while the conductance is defined on a semi-infinite interval ($g\geqslant 0$). In Figs. 8(b) ($E_\rangle$ polarization) and Fig. 8(d) ($H_\parallel$ polarization), we show the distribution of the logarithm of the conductance $p(\ln g)$ in the localized regime and observe that it is well approximated by a normal distribution for most of the domain. Thus in the localization regime g is log-normally distributed for both polarizations—a result that accords with its electronic counterpart. The exception to this is a sharp drop around $\ln g=0$. This drop is larger for $H_\parallel$ polarization than for $E_\parallel$ polarization, since the value of $\langle g\rangle$ is closer to the transition to Anderson localization for $H_\parallel$ polarization ($\langle g\rangle=0.1$) than for $E_\parallel$ polarization ($\langle g\rangle=0.029$). We expect a reduction of this drop when the number of layers in the stack is increased leading to a decrease of $\langle g\rangle$. Again these results are similar to those observed for electrons [5].

We turn now to the probability distribution for the transition regime. Previously, nonanalytic behavior of $p(g)$ near $\langle g\rangle=1$ was reported for electrons [9]. In Fig. 9, which displays the distributions $p(g)$ for average conductance values of $\langle g\rangle=0.98$ and 0.48, respectively, we see no evidence of nonanalytic behavior for $\langle g\rangle=0.98$ [Fig. 9(a)] in the vicinity of $g\approx 1$, but there the possibility exists of nonanalytic behavior for $\langle g\rangle=0.48$ [Fig. 9(b)], associated with the different slopes of the distribution on either side of $g\approx 1$. The behavior for $H_\parallel$ polarization in Fig. 10 is strikingly similar to that for $E_\parallel$ polarization.

We note that the probability density distribution at the transition in Figs. 9 and 10 is strikingly similar to that reported for the electronic case [5]. In both the electronic and photonic cases, the transfer matrices are symplectic (Refs. [5,26], respectively) and accordingly, in the spirit of random matrix theory, it is conceivable that their eigenvalue distributions, and the concomitant conductance probability distributions, may be similar.

To investigate in more detail the behavior of $p(g)$ near the transition $\langle g\rangle=1$, we present the logarithmic probability distribution in Fig. 11. The probability distribution $p(\ln g)$ has been calculated, assuming the absence of time reversal symmetry, by Muttalib *et al.* [9]. They derived

$$p(\ln g)\approx\sqrt{\frac{x\sinh 2x}{1-g}}e^{-\Gamma x^2}\quad \text{for } g<1, \tag{4}$$

$$p(\ln g)\approx\sqrt{2}ge^{-a(g-1)^2}\quad \text{for } g\geqslant 1, \tag{5}$$

where $x=\cosh^{-1}(1/\sqrt{g})$ and $\Gamma=\xi/N_L$. Here ξ is the localization length and a is a function of Γ [9]. Neither expression (4) nor (5) applies directly to this case which does exhibit time reversal symmetry. Nevertheless we have attempted a fit of our results (Fig. 11) with these approximate analytical results [9], since there are no known equivalents that apply to systems for samples with bulk defects with time reversal symmetry. Taking Γ to be a parameter chosen to optimize the fit, we obtain $\Gamma\approx 0.85$, a value somewhat different from $\Gamma=\xi/L\approx 0.47$ derived using our values for the localization length ξ and stack length N_L. Similarly for $H_\parallel$ polarization, the best fit to the data was obtained with $\Gamma\approx 0.85$ while the model gave $\Gamma=\xi/L\approx 0.76$. For both polarizations, the parameter $a\approx 14$. The presence of the logarithm function in Eqs. (4) and (5) provides evidence of a possible asymmetry in the slopes of the distribution to the left and to the right of $g\approx 1$. While this has been referred to in the literature [9], it should be regarded as a preliminary result in the context of our work. This is because the tails of the distributions are not sufficiently well characterized statistically, with the logarithm function exacerbating the problems by placing the un-

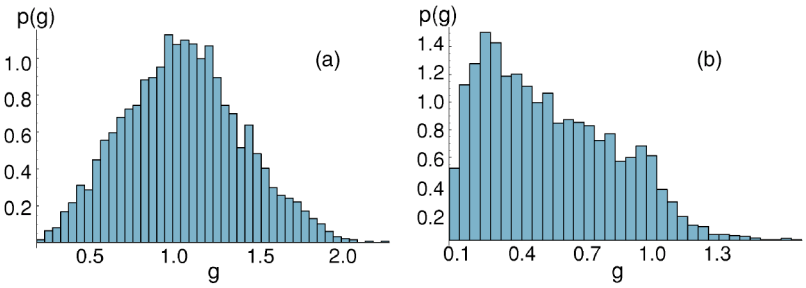

FIG. 10. Conductance distribution $p(g)$ at $\langle g\rangle=1.01$, $Q=1.5$, $N_L=20$ (a) and $\langle g\rangle=0.48$ $Q=1.5$, $N_L=30$ (b) for $H_\parallel$ polarization.

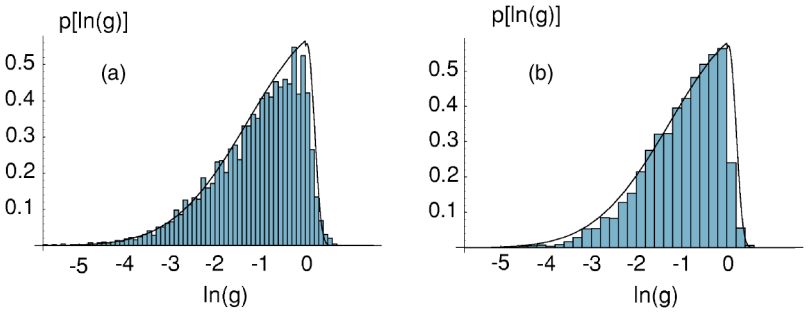

FIG. 11. Probability distribution for the logarithm of the conductance $p(\ln g)$ at $\langle g\rangle = 0.48$ for $E_{\|}$ (a) and $H_{\|}$ polarization (b). The fitting has been done by using Eqs. (4) and (5) and the given values of the parameters Γ and a.

resolved tails into the same bin. It is therefore possible that this apparent nonanalytic behavior might be a numerical artifact.

IV. CONCLUSION

In conclusion, we have calculated, using a high accuracy numerical method, the averaged conductance of a disordered, two-dimensional photonic crystal (comprising circular cylinders) for weak, moderate, and strong disorder. Of critical importance in these calculations is the inclusion of sufficiently many evanescent plane wave terms to ensure a well converged result. Substantial discrepancies can arise if only the propagating channels are included in the calculations.

Universal conductance fluctuations for photons have been explicitly demonstrated for $H_{\|}$ polarization in the case of weak and intermediate disorder. For $E_{\|}$ (TM) polarization, we have shown that the conductance variance is independent of sample size but is a strong function of disorder, with constant conductance fluctuations observed only in a very narrow region of disorder. Furthermore, where the $E_{\|}$ conductance variance is essentially constant, its value is identical to that for $H_{\|}$ polarization in the UCF region, with a value only slightly lower than the result predicted by random matrix theory for $\beta = 1$.

We have also shown that the conductance distributions are insensitive to polarization and show some indication of nonanalytic behavior. The distribution of the conductance at the transition to Anderson localization displays remarkable similarity for the two polarizations (Fig. 11). We also observe that $\langle g\rangle$ is more sensitive to the degree of disorder for $E_{\|}$ polarization than for $H_{\|}$ polarization. These findings merit further investigation, aimed at clarifying the essential similarities and differences between the behavior of photons and electrons in materials that have moderate to strong disorder.

ACKNOWLEDGMENTS

The work was produced with the assistance of the Australian Research Council. We also acknowledge computing support from the Australian Centre for Advanced Computing and Communication (ac3) and the Australian Partnership for Advanced Computing (APAC).

[1] P. A. Lee and A. D. Stone, Phys. Rev. Lett. **55**, 1622 (1985); B. L. Altschuler, JETP Lett. **41**, 648 (1985).
[2] *Mesoscopic Phenomena in Solids*, edited by B. L. Altshuler, P. A. Lee, and R. A. Webb (North-Holland, Amsterdam, 1991).
[3] E. Abrahams, P. W. Anderson, D. C. Licciardello, and T. V. Ramakrishnan, Phys. Rev. Lett. **42**, 673 (1979).
[4] B. Shapiro, Phys. Rev. B **34**, R4394 (1986).
[5] V. Plerou and Z. Wang, Phys. Rev. B **58**, 1967 (1998).
[6] P. Shengand and Z. Q. Zhang, J. Phys.: Condens. Matter **3**, 4257 (1991).
[7] P. Markos, Phys. Rev. Lett. **83**, 588 (1999); C. M. Soukoulis, X. Wang, Q. Li, and M. M. Sigalas, *ibid.* **82**, 668 (1999).
[8] M. Rühländer, P. Markos, and C. M. Soukoulis, Phys. Rev. B **64**, 212202 (2002).
[9] K. A. Muttalib and P. Wölfle, Phys. Rev. Lett. **83** 3013 (1999); K. A. Muttalib, P. Wölfle, A. Garcia-Martin, and V. A. Gopar, Europhys. Lett. **61**, 95 (2003).
[10] S. Feng, C. Kane, P. A. Lee, and A. D. Stone, Phys. Rev. Lett. **61**, 834 (1988); P. Sheng, *Scattering and Localization of Classical Waves in Random Media* (World Scientific, Singapore, 1990).
[11] J. A. Sanchez-Gil, V. Freilikher, A. A. Maradudin, and I. Yurkevich, Phys. Rev. B **59** 5915 (1999).
[12] A. Garcia-Martin and J. J. Saenz, Phys. Rev. Lett. **87**, 116603 (2001).
[13] Th. M. Nieuwenhuizen and M. C. W. van Rossum, Phys. Rev. Lett. **74**, 2674 (1995).
[14] E. Kogan and M. Kaveh, Phys. Rev. B **52** R3813 (1995).
[15] J. F. de Boer, M. C. W. van Rossum, M. P. van Albada, Th. M. Nieuwenhuizen, and Ad. Lagendijk, Phys. Rev. Lett. **73**, 2567 (1994).
[16] M. Stoytchev and A. Z. Genack, Phys. Rev. Lett. **79**, 309 (1997).
[17] P. A. Mello, P. Pereyra, and N. Kumar, Ann. Phys. (N.Y.) **181**, 290 (1988); O. N. Dorokhov, JETP Lett. **36**, 318 (1982); K. A. Muttalib, J.-L. Pichard, and A. D. Stone, Phys. Rev. Lett. **59**, 2475 (1987).
[18] L. C. Botten, N. A. Nicorovici, A. A. Asatryan, R. C. McPhedran, C. M. de Sterke, and P. A. Robinson, J. Opt. Soc. Am. A **17**, 2165 (2000); J. Opt. Soc. Am. A **17**, 2177 (2000).
[19] D. S. Fisher and P. A. Lee, Phys. Rev. B **23**, R6851 (1981).
[20] M. Büttiker, Y. Imry, R. Landauer, and S. Pinhas, Phys. Rev. B **31**, 6207 (1985).
[21] D. J. Thouless, in *Condensed Matter*, edited by R. Balian, R.

Maynard, and G. Toulouse (North-Holland, Amsterdam, 1979), p. 43.
[22] N. Giordano, Phys. Rev. B **38**, 4746 (1988).
[23] J. D. Joannopoulos, R. D. Meade, and J. N. Winn, *Photonic Crystals* (Princeton University Press, Princeton, NJ, 1995).
[24] C. W. Beenakker, Rev. Mod. Phys. **69**, 731 (1997).
[25] Y. Imry, *Introduction to Mesoscopic Physics* (Oxford University Press, Oxford, 2002).
[26] L. C. Botten, T. P. White, A. A. Asatryan, T. N. Langtry, C. Martijn de Sterke, and R. C. McPhedran, Phys. Rev. E **70**, 056606 (2004).